6-2015

The Effect of the El Nino-Southern Oscillation on U.S. Regional and Coastal Sea Level

B. D. Hamlington
Old Dominion University, bhamling@odu.edu

R. R. Leben

K. -Y. Kim

R. S. Nerem

L. P. Atkinson
Old Dominion University, latkinso@odu.edu

See next page for additional authors

Authors

B. D. Hamlington, R. R. Leben, K. -Y. Kim, R. S. Nerem, L. P. Atkinson, and P. R. Thompson

The effect of the El Niño-Southern Oscillation on U.S. regional and coastal sea level

B. D. Hamlington[1], R. R. Leben[2], K.-Y. Kim[3], R. S. Nerem[2], L. P. Atkinson[1], and P. R. Thompson[4]

[1]Center for Coastal Physical Oceanography, Old Dominion University, Norfolk, Virginia, USA, [2]Colorado Center for Astrodynamics Research, University of Colorado, Boulder, Colorado, USA, [3]School of Earth and Environmental Science, Seoul National University, Seoul, South Korea, [4]Department of Oceanography, University of Hawaii at Manoa, Honolulu, Hawaii, USA

Abstract Although much of the focus on future sea level rise concerns the long-term trend associated with anthropogenic warming, on shorter time scales, internal climate variability can contribute significantly to regional sea level. Such sea level variability should be taken into consideration when planning efforts to mitigate the effects of future sea level change. In this study, we quantify the contribution to regional sea level of the El Niño-Southern Oscillation (ENSO). Through cyclostationary empirical orthogonal function analysis (CSEOF) of the long reconstructed sea level data set and of a set of U.S. tide gauges, two global modes dominated by Pacific Ocean variability are identified and related to ENSO and, by extension, the Pacific Decadal Oscillation. By estimating the combined contribution of these two modes to regional sea level, we find that ENSO can contribute significantly on short time scales, with contributions of up to 20 cm along the west coast of the U.S. The CSEOF decomposition of the long tide gauge records around the U.S. highlights the influence of ENSO on the U.S. east coast. Tandem analyses of both the reconstructed and tide gauge records also examine the utility of the sea level reconstructions for near-coast studies.

1. Introduction

Rising sea levels threaten to permanently impact coastal infrastructure and ecosystems. In many coastal and island populations around the world, the effects of sea level rise are already being experienced [*Church et al.*, 2013]. While the impact of sea level change will be felt across the globe through the long-time scale inundation of coastal waters associated with secular global mean sea level rise, of similar concern for planning, adaptation, and mitigation efforts is the change in sea level occurring on shorter time scales. Such variations—considered here occurring on time scales ranging from interannual to decadal—have the potential to exacerbate the effects of the underlying trends in sea level by providing higher sea levels over which storms travel. Several recent studies have highlighted the potential for increased impact of storm surges superimposed on higher mean sea levels [*Cooper et al.*, 2008; *Kirshen et al.*, 2008; *Tebaldi et al.*, 2012; *Wahl et al.*, 2014]. Addressing and mitigating the effects of future changes in sea level thus involves not only accurately projecting future sea level rise, but also understanding and quantifying the additional contributions arising from internal variability.

The long-term secular trend in sea level is only one piece of the puzzle when considering sea level at a specific location at some point in the future. The regional sea level trends estimated over the satellite altimetry time period (from 1993 to present) are greater than 10 mm/yr in some locations and negative in others [*Cazenave and Llovel*, 2010; *Mitchum et al.*, 2010]. In particular, in the past 20 years, sea level has increased more than 20 cm in the western tropical Pacific, with some of this likely a result of decadal variability [e.g., *Merrifield et al.*, 2012] and some a result of anthropogenic forcing. On shorter time scales, the regional effect on sea level from internal climate variability could potentially exceed this 20 cm. Quantifying the contribution of internal variability and understanding the potential increases and decreases resulting from such variability on local levels becomes an important task when evaluating sea level risks, including those resulting from storm surge. This internal climate variability also serves to mask the underlying anthropogenic warming signal observed in sea level [e.g., *Meyssignac et al.*, 2012; *Hamlington et al.*, 2011a, 2014a]. By estimating and removing the contribution of internal variability to sea level, it is possible to gain an improved understanding of the underlying secular sea level trend and assess the possibility of an acceleration in sea level rise.

In this paper, we focus on the contribution of the El Niño-Southern Oscillation (ENSO) to regional and coastal sea level, with particular focus on the coastlines of the United States. To assess the impact of ENSO, we rely on cyclostationary empirical orthogonal function (CSEOF)-based global sea level reconstructions using over 20 years of satellite altimeter data and 60 years of tide gauge data. Through this analysis, the impact of the Pacific Decadal Oscillation (PDO), viewed here as low-frequency variability intrinsically related to ENSO, is also evaluated. While predicting and projecting the impacts of future ENSO events is a challenge, by examining the range of ENSO-related sea level variability over the past half-century, a general range can be placed on how much sea level rise or fall is expected to result from ENSO events in the future and how this is affected by the phase of low-frequency variability arising from the PDO. Constraining the possible effects of ENSO provides important information both for the near-term and long-term study of sea level.

2. Data

The modern satellite altimetry record spans only 22 years, making it difficult to separate longer-scale internal climate variability from secular trends and acceleration [e.g., *Church and White*, 2006, 2011; *Hamlington et al.*, 2011a; *Woodworth et al.*, 2009]. Historical measurements of sea level from tide gauges extend back as far as the beginning of the nineteenth century [*Holgate et al.*, 2013]. While providing long records, the measurements from tide gauges are generally sparse, particularly before 1950. However, by combining the dense spatial coverage of satellite altimetry with the long record length of the tide gauges, it is possible to reconstruct sea level on global scales to examine longer time scale climate signals and assess their contribution to sea level both regionally and globally [e.g., *Chambers et al.*, 2002; *Church et al.*, 2004; *Hamlington et al.*, 2011b; *Meyssignac et al.*, 2012]. Sea level reconstructions interpolate in situ tide gauge measurements (generally on a global scale) back in time using basis functions (i.e., spatial patterns) derived from satellite altimetry data or, in some cases, model data. The result is a data set with the spatial resolution of the satellite altimetry data, and the record length of the tide gauge data. In this paper, CSEOF reconstructed sea level from 1950 to 2010 [*Hamlington et al.*, 2011b, 2014b] is used. This data set is publicly available from the NASA/JPL Physical Oceanography Distributed Active Archive Center (PO.DAAC). The details of the reconstruction technique and resulting data set will not be described at length here, and the reader is referred to the cited references for additional information. For comparison and to examine the reconstructed data near the coasts, we also directly use and analyze the long-term tide gauge records spanning 1950 to present located along the coasts of the United States. We focus here on the U.S. coastlines as test case to evaluate the reconstruction near the coast, although future studies will involve the analysis of tide gauges on a wider scale. These monthly records were obtained from the Permanent Service for Mean Sea Level (PSMSL) and were used with minimal editing and filtering before performing the analysis. Finally, the Archiving, Validation and Interpretation of Satellite Oceanography (AVISO) merged multialtimeter sea surface height data from 1993 to present are used for comparison to the reconstructed sea level and to a set of tide gauge records.

3. CSEOF Analysis of Reconstructed Sea Level

The CSEOF method decomposes space-time data into a series of modes comprised of a spatial component (known hereafter as the loading vector (LV)), and a corresponding temporal component (known hereafter as the principal component time series (PCTS)) [*Kim et al.*, 1996; *Kim and North*, 1997]. The main difference between the CSEOF technique when compared to more traditional EOF analyses is that the CSEOF LVs are time varying over a specified nested period. The spatial patterns of many known phenomena in climate science and geophysics change in time with well-defined periods in addition to fluctuating at longer time scales. In other words, typical responses of a physical system are not stationary but evolve and change over time. By relaxing the stationarity imposed on EOF LVs, CSEOFs can provide a better representation of climate variability. CSEOFs also reduce mode mixing, which is a common problem with EOF decomposition.

In CSEOF analysis, the temporal evolution related to an inherent physical process is captured in the LV, while the corresponding PCTS explains the amplitude of this physical process through time. The nested period of the CSEOF analysis is selected a priori, with the decision usually based on some physical

understanding or intuition regarding the signal to be studied. When studying the annual signal known to be present in many geophysical data sets, for instance, a nested period of 1 year is chosen. The resulting LV would contain twelve spatial maps (when using monthly data) and would describe the physical evolution of the annual cycle through the year. In other words, for the northern hemisphere, the LV would show higher sea level in in the late summer months transitioning to lower sea level in the later winter months (see *Hamlington et al.* [2011a] for further details). The PCTS then describes the amplitude change—or strength—of the annual cycle from year to year.

In this study, a nested period of 2 years is selected for the CSEOF decomposition. This decision is based primarily on the biennial tendency of ENSO. *Rasmusson et al.* [1990] described warm (El Niño) and cold (La Niña) phases of ENSO as part of a biennial cycle that is modified by a lower-frequency mode with periods of 4–5 years. Here the goal is to capture the transition from the warm phase of ENSO to the cold phase of ENSO (and vice versa) in a single CSEOF mode, making the 2 year nested period a natural choice based on the *Rasmusson et al.* [1990] description. Two other studies—*Kim* [2002] and *Yeo and Kim* [2014]—provide a more detailed study of the nested period and established a physical explanation for extracting tropical Pacific Ocean variability with a 2 year nested period. Particularly relevant for the present study, *Yeo and Kim* [2014] find that with a 2 year CSEOF decomposition of 140 years of sea surface temperature (SST), two dominant global modes of variability focused primarily in the tropical Pacific are obtained and subsequently relate to ENSO. The first mode describes low-frequency variability in the Pacific Ocean, signifying a link between the tropical Pacific and northern Pacific on interannual to decadal time scales. Furthermore, the PCTS of this mode shows a strong correlation with the PDO index over the full record. The second CSEOF mode represents the biennial oscillation of ENSO with the LV capturing the phase transition between El Niño and La Niña events. The PCTS of this mode exhibits variations with a period of roughly 4–5 years, likely representing the low-frequency modulation of the biennial oscillation described in *Rasmusson et al.* [1990].

The goal of this study is to obtain two similar CSEOF modes from reconstructed sea level. As a first step, a CSEOF decomposition using a 2 year nested period of the 60 year reconstructed sea level data is conducted. The first two global CSEOF modes after removing the trend (the least squares estimated trend at each data point is removed prior to decomposition) explain 22% and 18% of the variance, respectively. In order to obtain sea level modes describing similar variability as those found from the SST record, we rely on CSEOF regression analysis (demonstrated in, for example, *Yeo and Kim* [2014]). This regression technique provides CSEOF sea level modes that are related to corresponding CSEOF SST modes. In other words, the analysis creates regressed sea level CSEOF LVs that have the same temporal evolution (PCTS) as the two SST modes obtained in *Yeo and Kim* [2014]. Although the regression forces the LVs to have the same (or similar) PCTS, it does not dictate that the resulting LVs be in phase. On the contrary, the phase information of the LVs is built into the analysis through this regression, a significant advantage over other analysis/decomposition techniques. Since the LVs change in time over the nested period, the CSEOFs provide for the possibility of one variable leading the other in the evolution of ENSO. The resulting set of LVs are said to be physically consistent and, assuming a regression relationship can be established, are analyzed in tandem to gain information about the signal or system of interest. The following steps outline the procedure for obtaining LVs in one variable (in this case sea level, the predictor, labeled with subscript P) that have the same PCTS as another variable (in this case SST the target, labeled with subscript T):

1. Perform CSEOF decompositions of the target variable and the predictor variable over a common time period.

2. Regress all predictor *PCTS* (in this study, $i = 1:i_{max}$, with $i_{max} = 20$) on each individual target *PCTS* ($n = 1:n_{max}$, with $n_{max} = 2$ in present study for the two modes shown in Figures 1 and 2), to compute a set of regression coefficients, α:

$$PCTS_{T,n}(t) = \sum_i \alpha_{i,n} PCTS_{P,i}(t) + \varepsilon(t) \tag{1}$$

3. Use the regression coefficients computed in (2), along with the original predictor loading vectors, LV_P, to form the regressed predictor variable spatial patterns, LVR_P *(r, t)*, with amplitude fluctuations described by $PCTS_T(t)$:
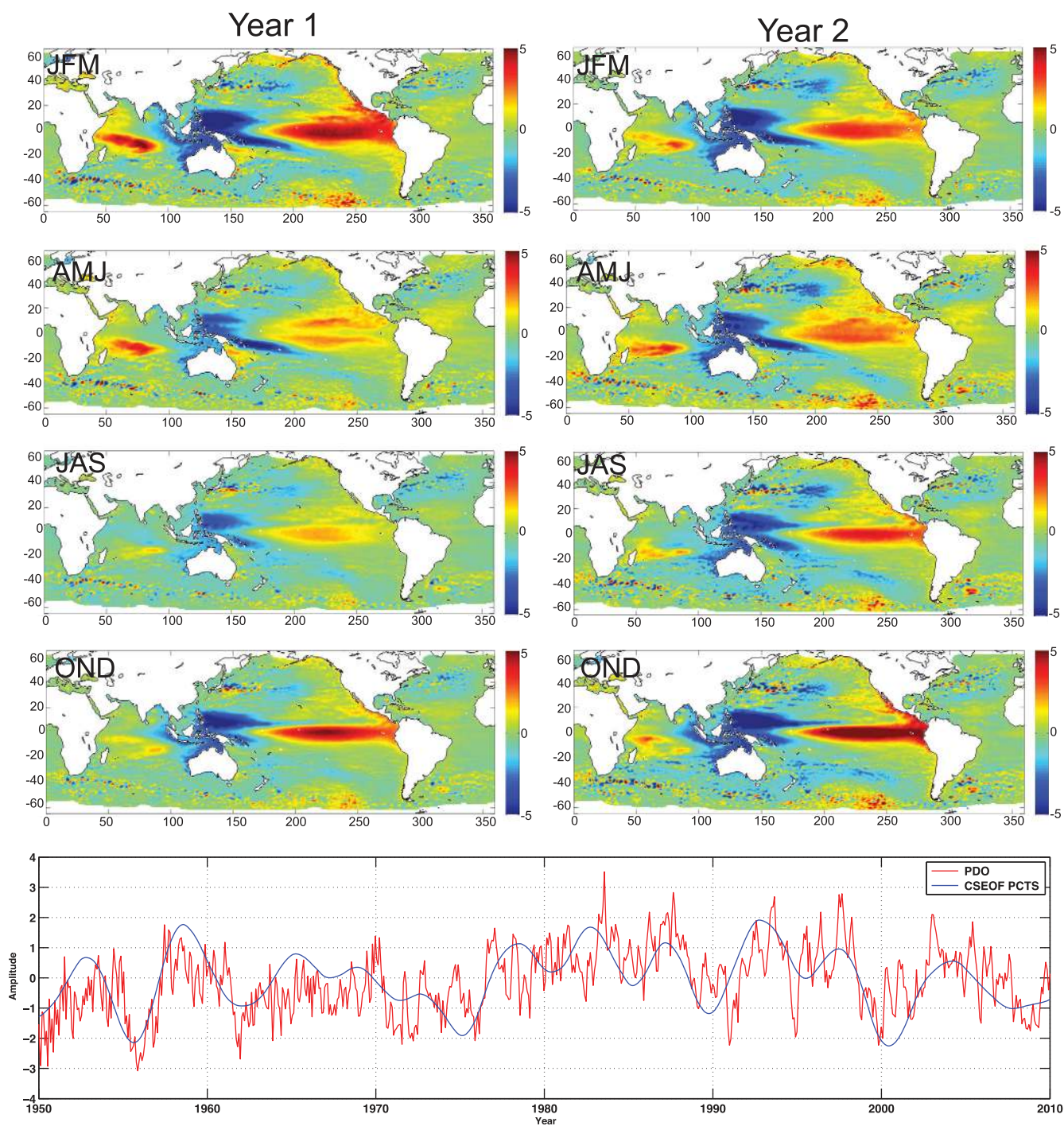
Figure 1. Regressed CSEOF sea level mode from a 2 year nested period decomposition representing the low-frequency ENSO variability. (Top) The averaged seasonal LVs for years 1 and 2 (units of cm) and (bottom) the corresponding PCTS (dimensionless), with the PDO index shown for comparison.

$$LVR_{P,n}(r,t) = \sum \alpha_{i,n} LV_{P,i}(r,t) \qquad (2)$$

After performing the same CSEOF decomposition of the Extended Reconstruction SST [*Smith et al.*, 2008] as done in *Yeo and Kim* [2014], we regress the 2 year CSEOF reconstructed sea level modes on to the first two SST modes. In total, 20 CSEOF sea level modes are used in the regression. Beyond this number, the regression procedure begins to over fit the data and leads to the addition of noise in the regressed LVs. The
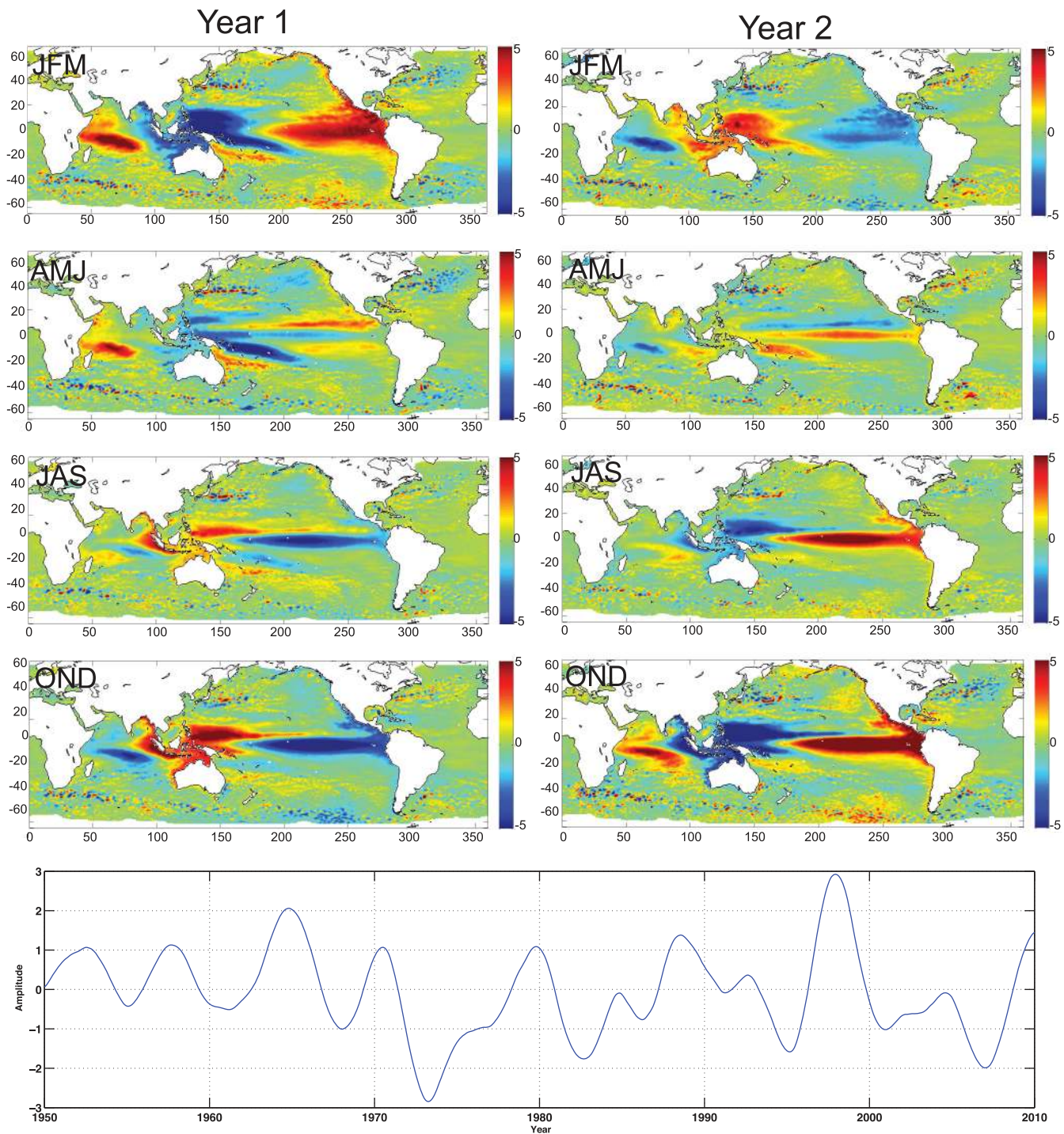
Figure 2. Comparison of PDO computed from (a) AVISO data, and (b) CSEOF sea level reconstruction (units of cm). PDO is defined here to be the first (dominant) EOF of northern Pacific sea level variability. (c) The corresponding PCTS (dimensionless) for AVISO (red) and the reconstruction (black), along with the PDO index for comparison (blue).

resulting two regressed CSEOF modes are shown in Figures 1 and 2. The spatial pattern of the first CSEOF mode does not vary significantly across the 2 year nested period, reflecting the low-frequency nature of the variability captured in this mode (Figure 1). The sea level pattern in the tropical and equatorial Pacific is similar to the well-known ENSO signal, with strong positive sea level values over the tropical eastern and central Pacific. There is, however, significant variability in the North Pacific, with the spatial pattern showing a

similar structure to the PDO [*Mantua et al.*, 1997; *Mantua and Hare*, 2002; *Cummins et al.*, 2005]. More specifically, in its positive phase (shown in the LVs of Figure 1), higher sea level near the coastlines wraps around a core of lower sea level in the north central Pacific. Indeed, the PCTS of this mode shows a strong correlation of 0.80 with the 2 year moving average of the monthly PDO index. Several studies have recently suggested that the low-frequency variability of ENSO is modulated by decadal variability (PDO) in the north Pacific [*Gu and Philander*, 1997; *Latif et al.*, 1997; *Barnett et al.*, 1999; *Kleeman et al.*, 1999; *Pierce et al.*, 2000; *Vimont et al.*, 2003]. As with the SST mode in *Yeo and Kim* [2014], the CSEOF sea level mode likely represents the link between the tropical Pacific and the north Pacific—and by extension the link between ENSO and the PDO—on long time scales. While the argument could be made that this mode should be referred to as the PDO, the sea level mode extracted here is global in scale whereas the PDO is by definition constrained to the northern Pacific Ocean. More specifically, the PDO is defined to be the first EOF mode of either north Pacific SST [e.g., *Mantua and Hare*, 2002] or north Pacific sea level [e.g., *Cummins et al.*, 2005]. For comparison and verification that the sea level reconstruction captures this variability, the first EOF is computed from both AVISO and sea level reconstruction data using only data from the northeast Pacific (as defined in *Cummins et al.* [2005]). The two modes agree very well both spatially and temporally (Figure 2), with the agreement improving when the EOF decompositions are computed from data sets using only data from the overlapping time period. Comparing the EOF LV to the same region in Figure 1 finds a similar spatial pattern albeit with a slightly smaller amplitude in the reconstruction, which likely results from computing the modes over disparate regions with differing variability. For ease of discussion and to distinguish the global mode (Figure 1) from the regional PDO mode (Figure 2), the global mode will be referred to as an ENSO mode and will be interpreted as representative of the low-frequency variability of ENSO.

The second CSEOF mode (Figure 3), on the other hand, depicts the biennial oscillation between positive and negative ENSO events. The maximum amplitude is found at the end of the calendar year, with the preceding months capturing the buildup to the warm and cold events (following the description in *Rasmusson et al.* [1990] and others). The PCTS clearly shows the strong ENSO events in 1972/1973, 1982/1983, and 1997/1998 (note the sign for the 1972/1973 and 1982/1983 El Niño events is negative in the PCTS as it begins on an even year rather than an odd year, an artifact of the 2 year nested period). In addition to strong variability in the tropical Pacific, the Indian Ocean also shows a pattern consistent with the Indian Ocean Dipole [e.g., *Saji et al.*, 1999] and/or the Indian Ocean Subtropical Dipole [e.g., *Suzuki et al.*, 2004] that is oscillating with a similar 2 year frequency. While the variability associated with the Indian Ocean will not be discussed at length here, the variability exhibited by this mode outside of the Pacific Ocean highlights its global nature.

4. The Contribution of ENSO to Regional Sea Level

Having extracted two independent modes explaining internal variability in the Pacific Ocean related to ENSO across a range of time scales, the contribution of ENSO to regional sea level over the past 60 years can be assessed. Since the goal is to identify general ranges of possible sea level contributions, extensive error estimates and discussion thereof are beyond the intentions of this paper and will not be presented. Error in the sea level reconstruction is discussed in *Hamlington et al.* [2011b], and the large values (tens of centimeters) given here are much larger than the associated error, particularly for the dominant modes of variability like ENSO in the reconstructed data set. To quantify the possible range of ENSO-related sea level change, the maximum and minimum value in the last 60 years resulting from each mode is evaluated at every location across the globe to establish a range of possible sea level values. Figure 4 shows the spatial patterns for the maximum and minimum values for the combined modes (a and b) in addition to the contributions from modes 1 (c and d) and 2 (e and f) individually. In the tropical Pacific, the maximum and minimum values of modes 1 and 2 have very similar spatial patterns. However, the maximum contribution to sea level is generally lower for the low-frequency mode when compared to the contribution from the biennial mode. In the eastern Pacific, the biennial CSEOF ENSO mode is associated with almost half a meter of sea level change in the deep ocean of the eastern equatorial Pacific, with values approaching 30 cm for islands in the western Pacific and coastlines of South America. Additionally, mode 2 has a much larger sea level signal along the west coasts of North and South America. Depending on the phase, it is possible for the signals captured by the two modes to constructively or destructively combine. To evaluate the combined contribution, the two modes are first summed and then the maximum and minimum values for the last 60 years at each location are computed. As seen in Figures 4a and 4b, peak to peak values in the eastern Pacific are larger than either of the individual
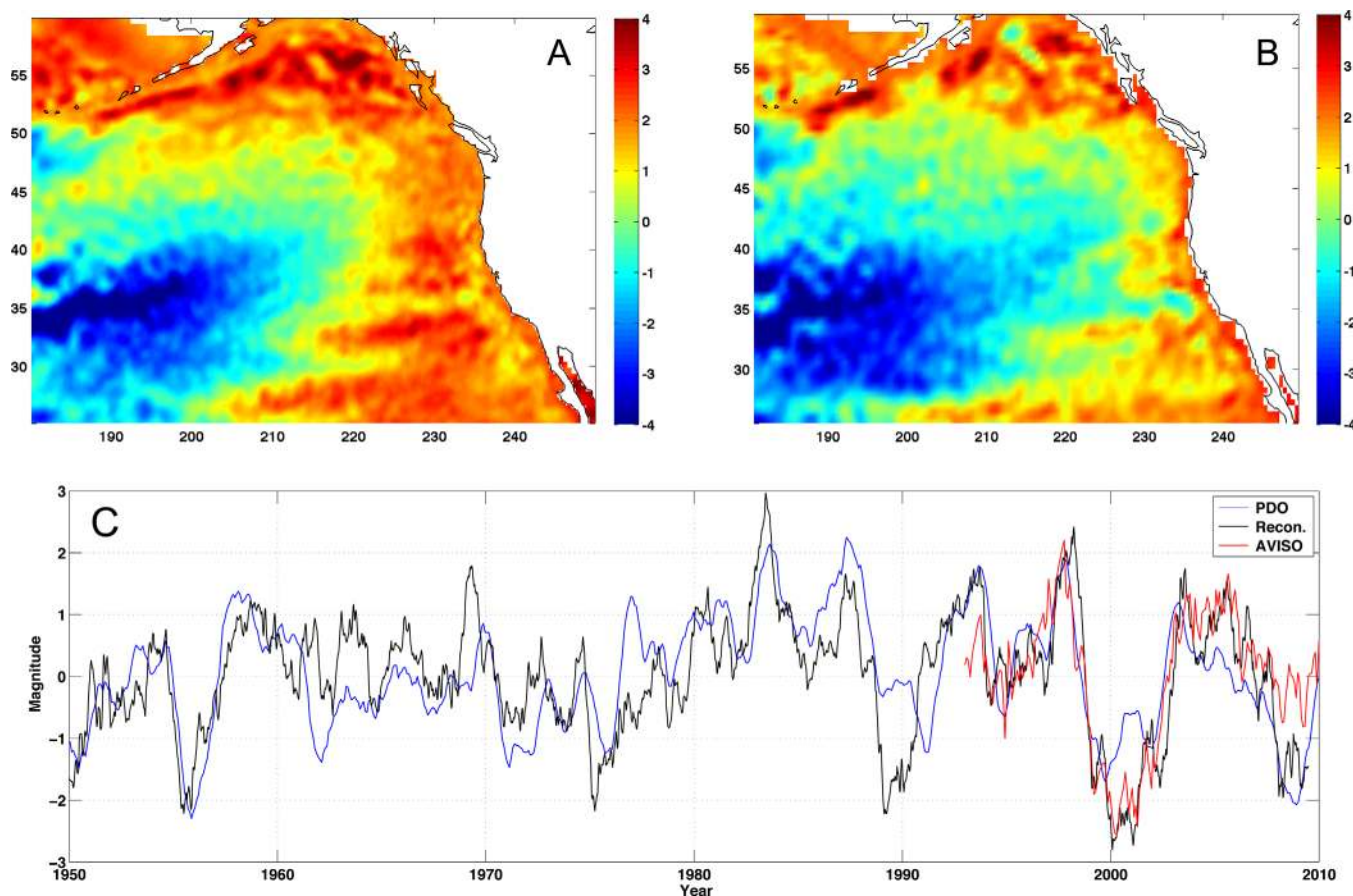
Figure 3. Regressed CSEOF sea level mode from a 2 year nested period decomposition representing the biennial oscillation of ENSO. (top) The averaged seasonal LVs for years 1 and 2 (units of cm) and (bottom) the corresponding PCTS (dimensionless).

mode contributions. When the two modes combine in a constructive manner, regional sea levels in the equatorial and tropical Pacific can increase or decrease upward of 60 cm on relatively short time scales. Furthermore, sea level along the U.S. west coast can increase on the order of 20 cm.

At this point, it should be noted that it is possible that not all of the ENSO variability is captured in the two modes shown in Figures 1 and 3. Recent studies have suggested that several modes are needed to capture the full spectrum of ENSO variability [e.g., *Compo and Sardeshmukh*, 2010]. However, the interannual-to-decadal variability associated with ENSO does appear to be well captured in these two modes. To test this, we computed the variance explained by these two modes at each point across the globe. In many locations in the tropical Pacific, these two modes explain near 80% of the total reconstructed sea level variance (Figure 5). Additionally, computing the Niño-3.4 index from the total sea level reconstruction and from the leading two modes shows that the large sea level change associated with the strong ENSO events is almost entirely captured by the first two modes (Figure 5b). These two tests combined with previous comparisons of the sea level reconstruction and satellite altimeter data [*Hamlington et al.*, 2011b] provide confidence that we are capturing the majority of the ENSO variability in the reconstruction on the time scales of interest and in the study region, although further tests need to be conducted regarding whether other regions of the world are similarly well explained.

5. Contribution of ENSO to Coastal Sea Level

We have estimated the ENSO-induced sea level change on basin-wide scales; however, the potential contribution of ENSO to sea level change near the coast may be perhaps of greater importance. By focusing on
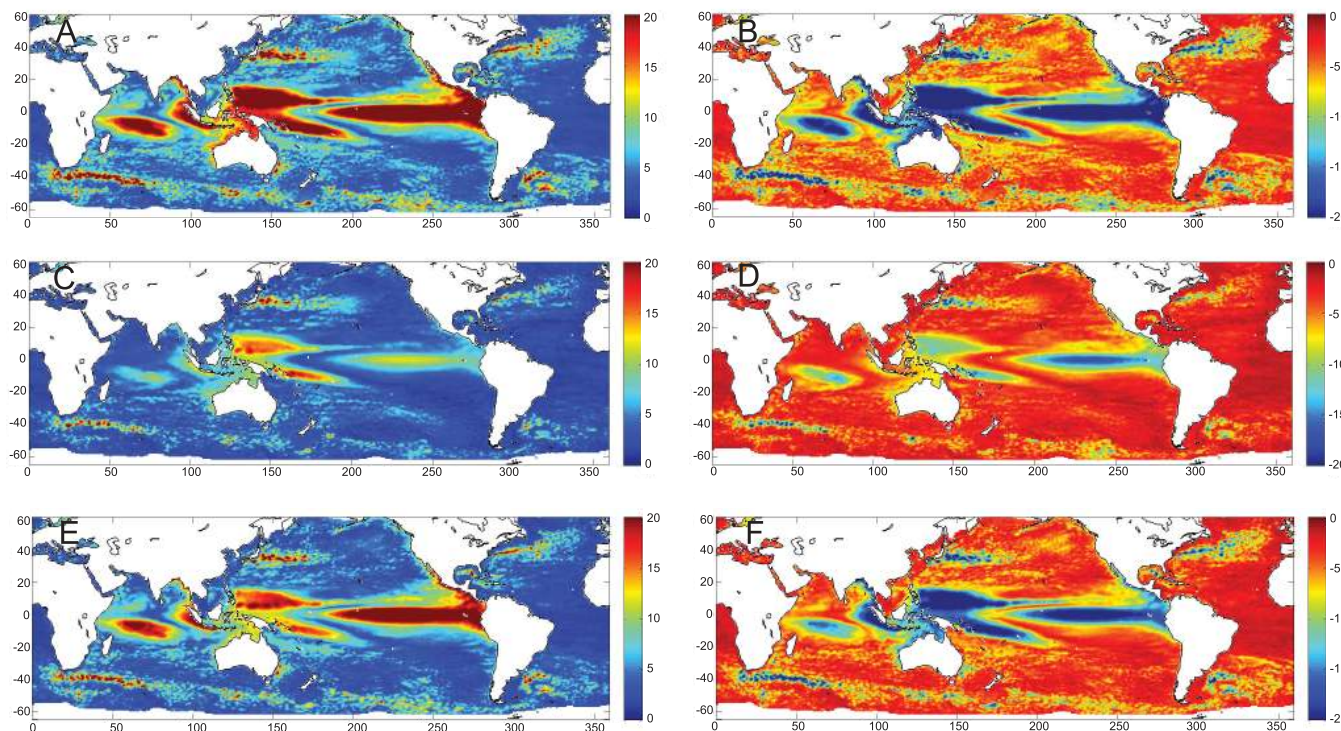
Figure 4. (left) Maximum and (right) minimum contributions to regional sea level from 1950 to 2010, for (middle) first mode only, (bottom) second mode only, and (top) combined first and second modes. Units are in centimeters.

the west and east coasts of the United States, we not only estimate the ENSO-induced sea level change along these coastlines but also evaluate the utility of the reconstruction for near-coast applications in general. There are two potential problems with sea level reconstructions near the coasts: (1) the accuracy of the satellite altimeter data upon which the reconstruction is based decreases when approaching the coast for a number reasons, including the inadequacy of corrections (e.g., wet troposphere, tides, etc.) near the coast, difficulties in estimating the mean sea level over the continental slope and shelf, and issues of land contamination in the altimeter and radiometer footprints near the coast; and (2) how well the tide gauges represent the interior/deep ocean signal and vice versa [e.g., *Vinogradov and Ponte*, 2011]. To date, there have been no comprehensive studies using sea level reconstructions to study coastal sea level signals. A combination of altimetry, tide gauge and sea level reconstruction data, is useful, therefore, to both quantify the ENSO contribution to sea level along the coasts of the United States and evaluate the quality of the reconstruction near the coast.

Sea level change and the associated trends along the coasts of the United States have been the focus of several recent studies [e.g., *Merrifield et al.*, 2012; *Bromirski et al.*, 2011; *Zhang and Church*, 2012; *Moon et al.*, 2013; *Thompson et al.*, 2014; *Thompson and Mitchum*, 2014; *Woodworth et al.*, 2014]. During the satellite altimeter record, trends off the U.S. west coast have been flat and generally lower than the trend in global mean sea level [*Bromirski et al.*, 2011]. Sea level along the Pacific coast of North America is correlated with ENSO and the PDO [*Enfield and Allen*, 1980; *Chelton and Davis*, 1982; *Cummins et al.*, 2005]. Using the CSEOF analysis conducted here, we can begin to assess the combined contribution of the two independent modes related to ENSO across a range of time scales. As a first check, the combined contribution of the two modes shown in Figures 1 and 3 is estimated at the nearest point to three west coast tide gauges with records spanning the entire reconstruction time period. In Figure 6, the ENSO contribution from the two modes is compared to both the tide gauge data (detrended over the full record available at each gauge, annual cycle removed, inverted barometer correction applied) and AVISO satellite altimetry data (detrended, annual cycle removed, inverted barometer correction applied) for the tide gauges in San Francisco (a), San Diego (b), and Crescent City (c). For each of the three locations, the contribution of the ENSO modes agrees very
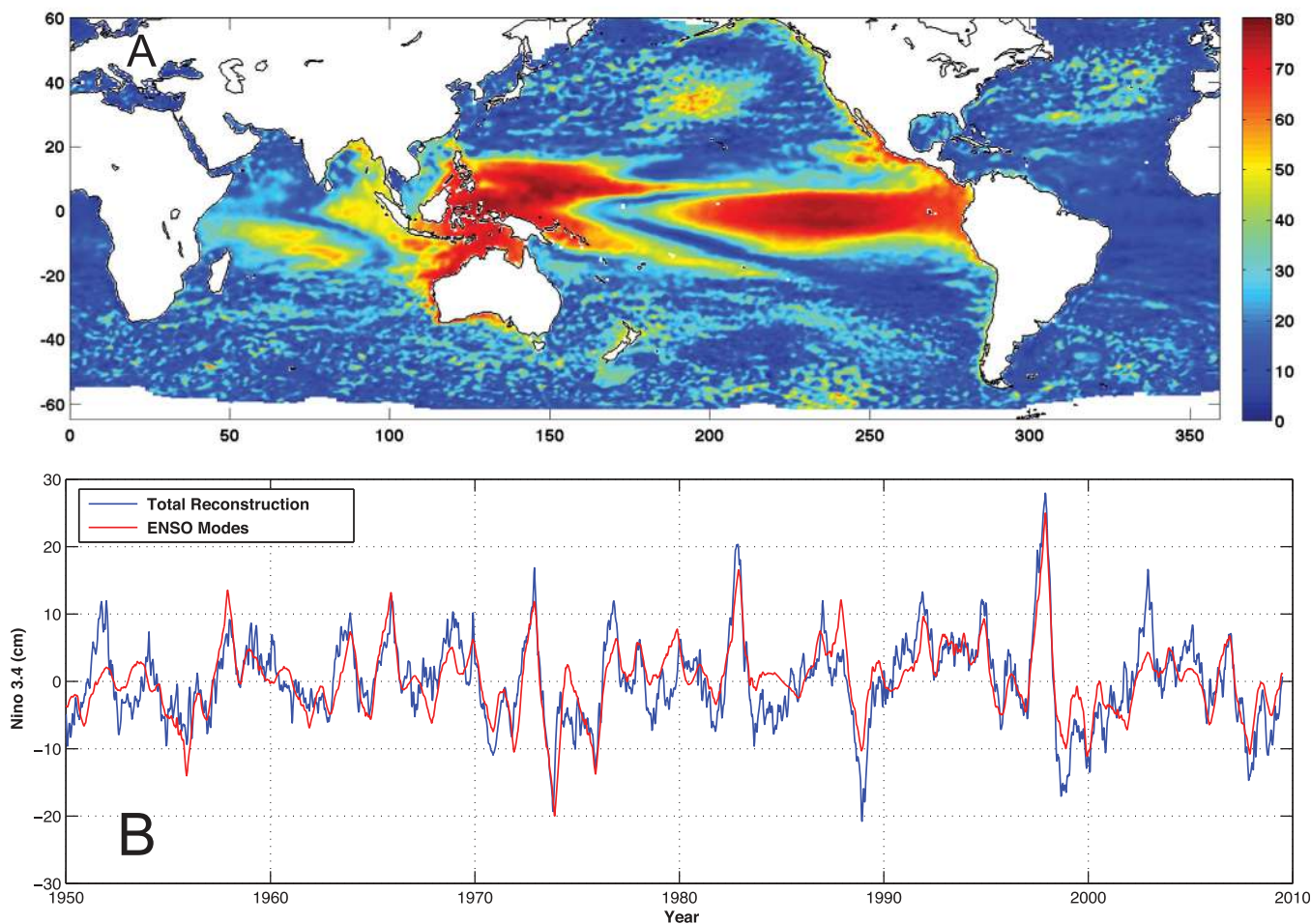
Figure 5. Percentage of variance explained in original reconstructed data set by combined ENSO modes. (b) Sea level analogue of the temperature-based Nino-3.4 index computed from combined ENSO modes (red) and full reconstructed sea level data set.

well with the AVISO satellite altimetry with the two showing very similar amplitudes for the 1997/1998 El Niño. Both the reconstructed ENSO modes and AVISO satellite altimetry data, however, show reduced amplitudes when compared to the tide gauge data. This is particularly apparent in the comparison between the reconstruction and tide gauges for the 1982/1983 El Niño, which was at least as large in the tide gauge records as the 1997/1998 event. There are a number of reasons why this discrepancy between the tide gauge data and reconstruction/altimetry may exist. Perhaps the simplest explanation is the difference in location between the tide gauge and the nearest point in the sea level reconstruction. The sea level reconstruction does not extend all the way to the coastline and is computed on a half-degree grid that does not provide data at the exact location of the tide gauge. The inability to extend the reconstruction closer to the coast with a higher resolution than provided by a half-degree grid could also result in missing variability associated with near-coast oceanographic processes. As another possibility, global modes might not be able to fully explain regional variability and a more targeted regional analysis made lead to improvement. Finally, as suggested above, it is also possible that the sea level measurements from the altimetry are not representative of the tide gauge record. This could result from errors in the altimetry measurement or processing of the AVISO data product near the coast, but more likely is the result of differences between the local sea level response to ENSO at the tide gauges and the open/deep ocean response measured by the altimetry, and thus captured in the reconstruction. Using a spectral approach, *Subbotina et al.* [2001] showed that both the 1982/1983 and 1997/1998 El Niño gave rise to enhanced sea level variability at west coast tide gauges at periods of days to weeks because of passing atmospheric systems. Further, they found
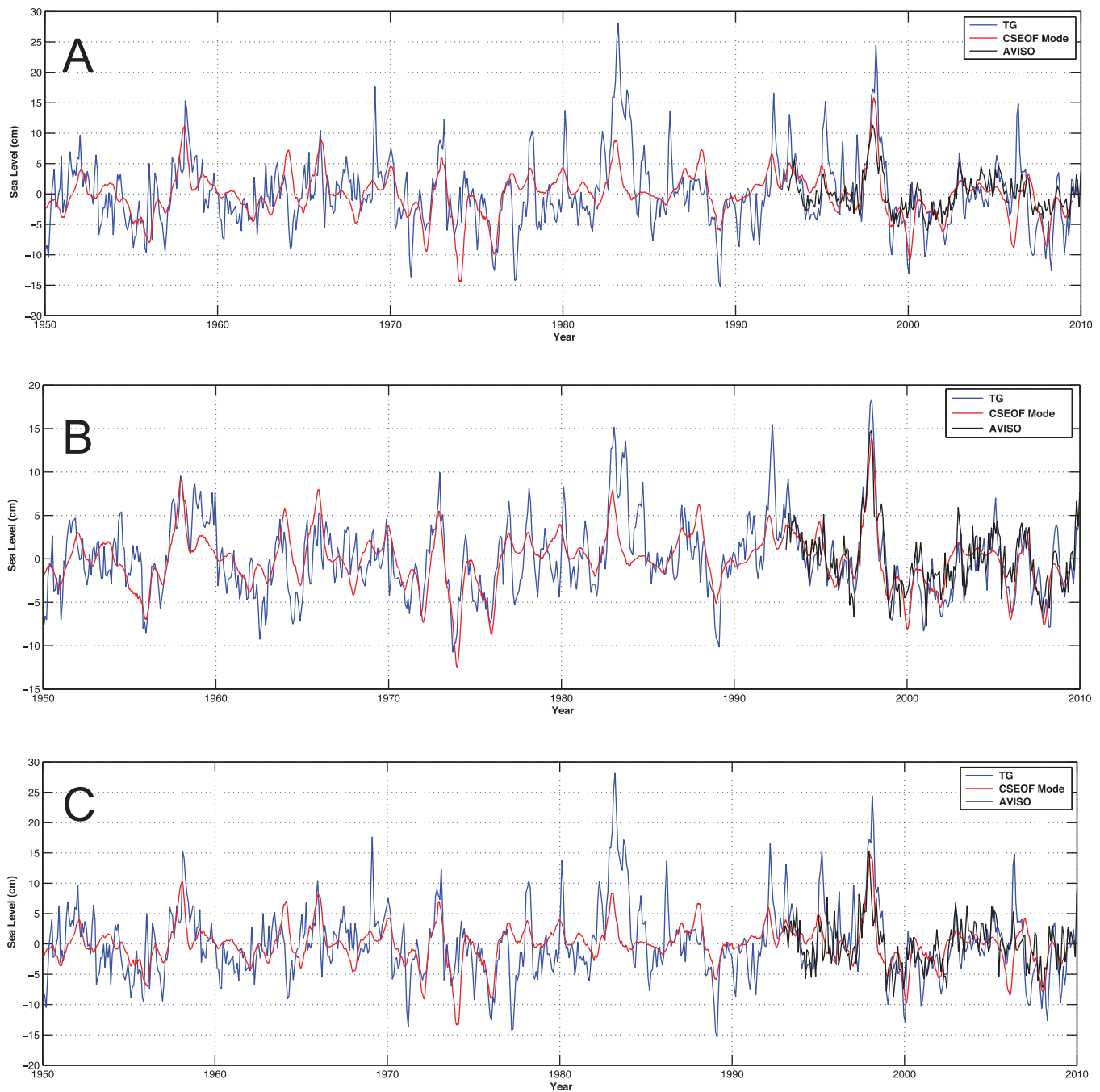
Figure 6. Comparison between the tide gauge data, 2 year ENSO mode contribution from the sea level reconstruction, and AVISO data for the tide gauges of (a) San Francisco, (b) San Diego, and (c) Crescent City. For the AVISO data and reconstruction, the nearest data point to the actual tide gauge location is used. Data are detrended and the inverted barometer correction has been applied to the tide gauge and AVISO data.

that much of the sea level variability observed at mid to high latitudes along the west coast was associated with an atmospheric teleconnection that gave rise to amplifications in coastal sea level pressure and wind stress. Based on the conclusions of this study, the response to ENSO on coastal sea level is inextricably tied to the open ocean signal as captured by the reconstructed ENSO modes shown in Figures 1 and 3, but the actual change in sea level at the coast during an ENSO event can be enhanced by synoptic-scale atmospheric variability and coastally linked processes.
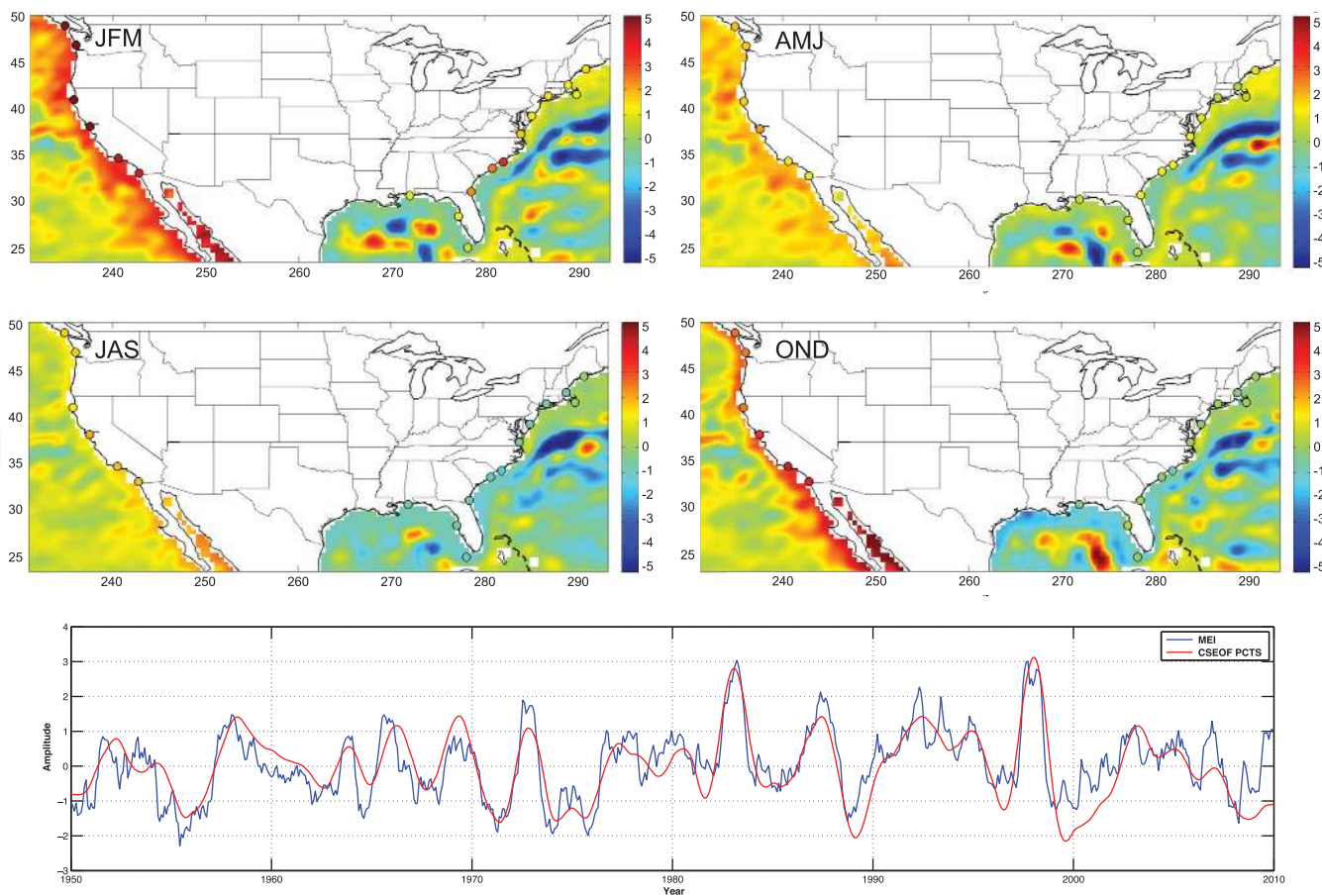
Figure 7. ENSO CSEOF mode (units of centimeters) obtained using a 1 year decomposition of the sea level reconstruction (background) and U.S. coastal tide gauge data (overlaying filled circles). Seasonally averaged LV patterns are provided in the top plots with the corresponding PCTS shown in the bottom plot. The MEI is shown for comparison to the PCTS.

To further address the discrepancy in the coastal ENSO signal observed by the tide gauges and the sea level reconstruction, CSEOF decompositions are performed directly on the long tide gauge records available along the coasts (both east and west) of the United States. Only tide gauge records with small gaps during the 60 year time period from 1950 to present were used, and as necessitated by the CSEOF technique, these small gaps were filled using simple linear interpolation. The resulting tide gauges were first decomposed using CSEOF analysis with a 1 year nested period. This 1 year nested period was the same as that used to create the original reconstruction (see *Hamlington et al.* [2014b] for more details) and provides a simple comparison between the reconstruction and the tide gauges. The first CSEOF mode in the reconstruction has been linked to the conventional eastern-Pacific ENSO in several previous studies [e.g., *Hamlington et al.,* 2011a, 2013, 2014b]. The first CSEOF PCTS from the tide gauges has a correlation of 0.79 with the first PCTS from the reconstruction, but to make a direct comparison, the tide gauge PCTS are regressed on to the first sea level reconstruction PCTS. This allows for easier comparison of the CSEOF LVs from the two sets of data since they will then have the same PCTS (or more exactly, similar PCTS given the limits of the regression which provides a correlation of 0.98). The seasonal CSEOF LVs for the reconstruction (background) and tide gauges (filled circles around the coastlines) are shown in the top plots of Figure 7. In the bottom plot of Figure 7, the PCTS explaining the temporal variation of these spatial patterns is shown and compared to the Multivariate ENSO Index (MEI) [*Wolter et al.,* 2011]. In January-February-March (JFM), the tide gauge-based CSEOF LV shows stronger amplitudes than the reconstruction-based CSEOF LV. In particular, the ENSO-related signal at higher latitudes along the west coast is generally smaller in the reconstruction than in the tide gauges. Additionally, the east coast tide gauges are observed to have a signal associated with ENSO that is not similarly captured by the reconstruction. This difference between the tide gauge LV and
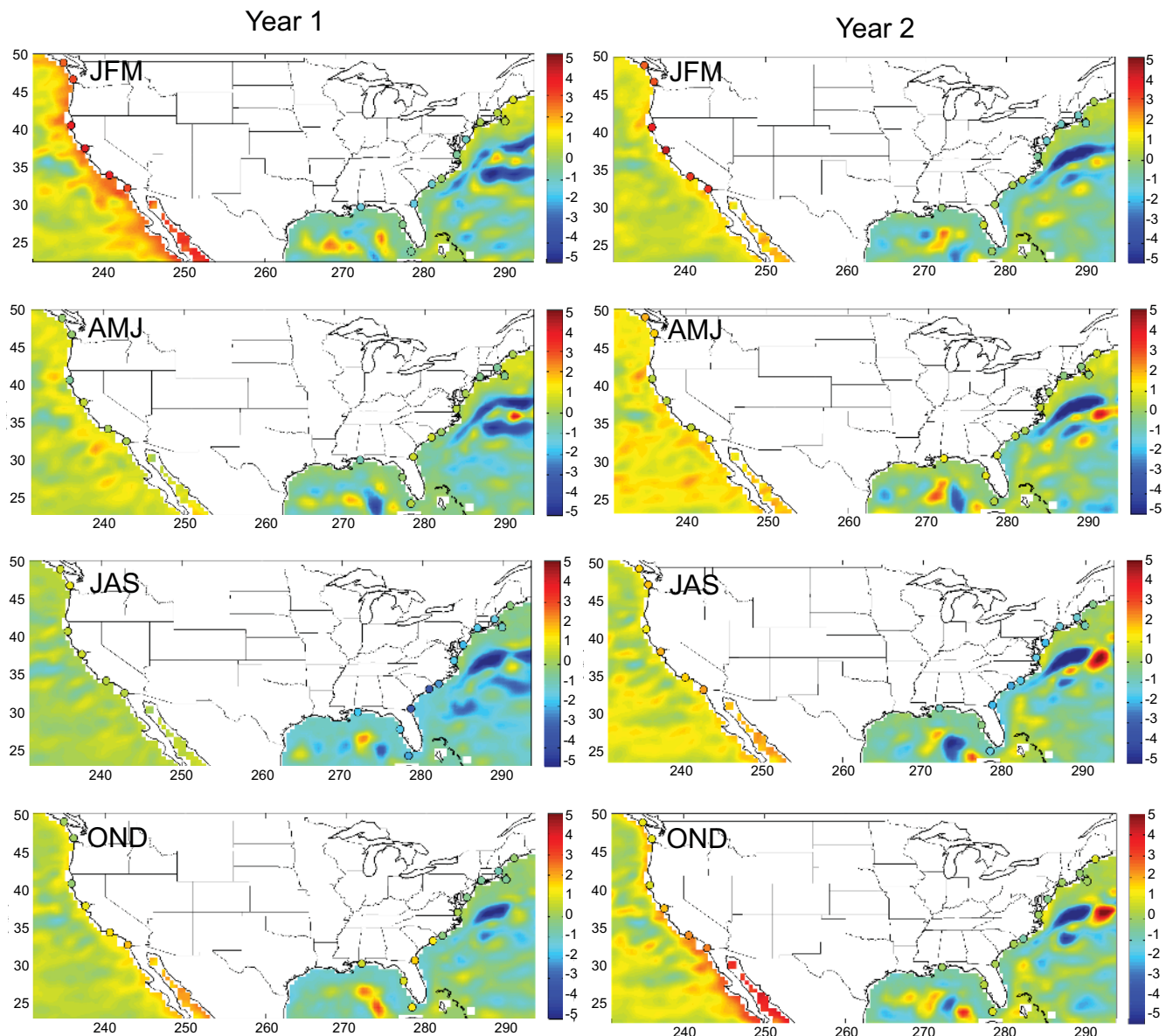
Figure 8. Low-frequency ENSO CSEOF mode obtained using a 2 year decomposition of the sea level reconstruction (background, as in Figure 1) and U.S. coastal tide gauge data (overlaying filled circles). The corresponding PCTS is shown in Figure 1.

reconstruction LV in JFM explains, in part, the discrepancy shown in Figure 6. In the other three seasons, the correspondence between the tide gauge LV and reconstruction LV is much better. The two LVs also provide information regarding the lag in the ENSO-signal between the east and west coast. While the ENSO signal along the west coast in October-November-December (OND) strengthens considerably, the east coast ENSO signal is negligible before subsequently strengthening in JFM. There also appears to be a distinction between the ENSO-related signals north and south of Cape Hatteras, with the area to the south more heavily affected by ENSO-related sea level variability (similar results were obtained in *Sweet and Park* [2014]). Similar to the study of *Subbotina et al.* [2001] along the west coast, a number of other studies have looked at the link between ENSO and sea level variability at the tide gauges located along the southeast coast noting the increased storminess that occurs along the east coast as a result of ENSO-related variability [e.g., *Sweet and Zervas*, 2011; *Thompson et al.*, 2013]. This increased storminess along the southeast coast discussed in these studies provides an explanation for the discrepancy between the tide gauges and
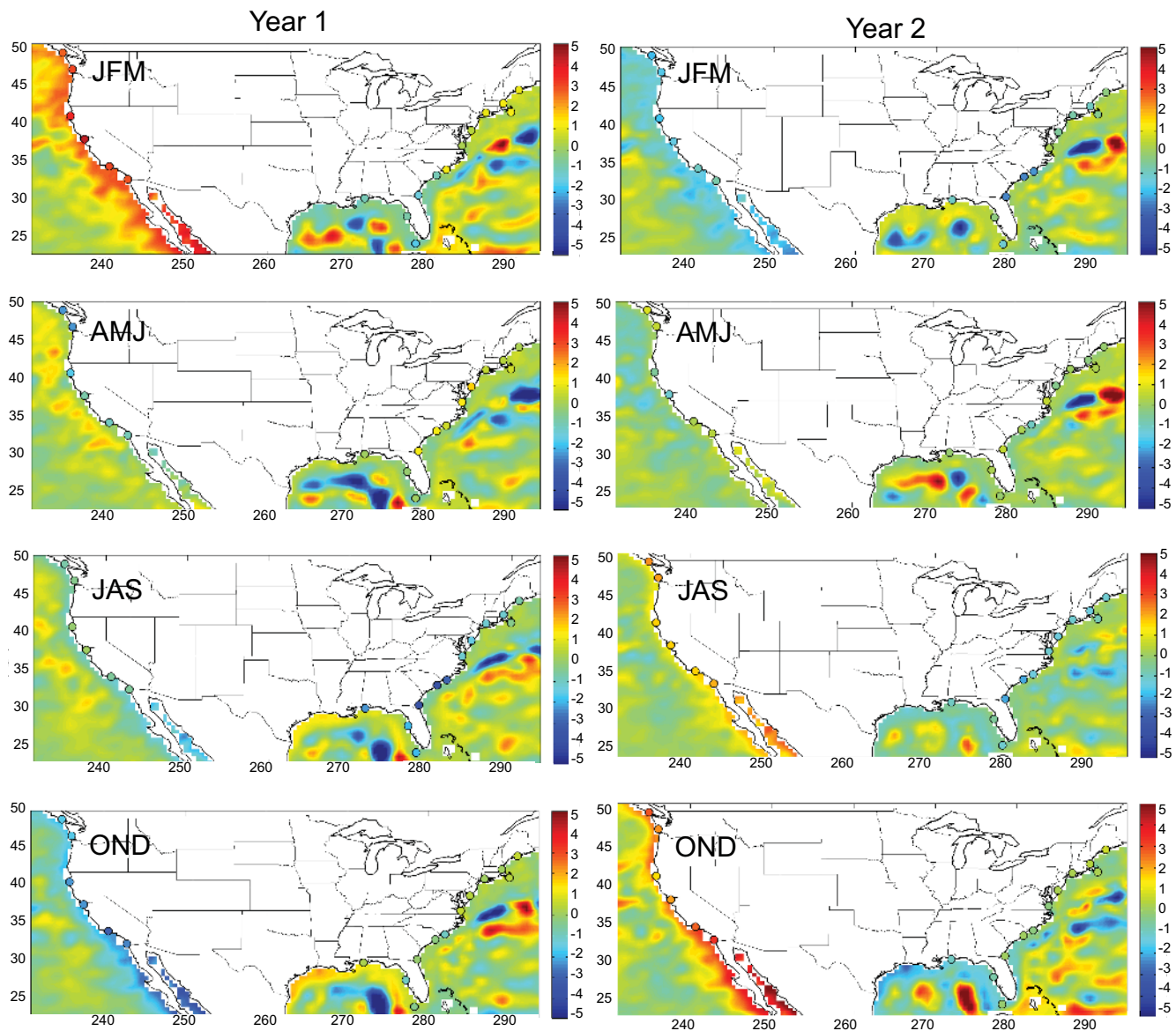
Figure 9. Biennial oscillation ENSO CSEOF obtained using a 2 year decomposition of the sea level reconstruction (background, as in Figure 2) and U.S. coastal tide gauge data (overlaying filled circles). The corresponding PCTS is shown in Figure 2.

reconstruction, as the short-term sea level variability associated with storms is unlikely to be captured by the global patterns from satellite altimetry that serve as the basis for the reconstruction.

To compare the tide gauge data to the 2 year ENSO modes shown in Figures 1 and 3, a 2 year CSEOF decomposition was conducted on the west and east coast tide gauges. The 2 year tide gauge LVs were then regressed on the PCTS from the low-frequency and biennial oscillation ENSO modes to allow for direct comparison between the reconstruction and tide gauges. The resulting LVs from the tide gauges are shown in comparison to the reconstructed modes in Figure 8 (low-frequency ENSO mode) and Figure 9 (biennial oscillation ENSO mode). The corresponding PCTS for these two modes are given in Figures 1 and 3, respectively. For the biennial oscillation mode (Figure 9), the agreement between the tide gauges and reconstruction is excellent throughout the 2 year period of the LV. Both sets of data exhibit an oscillation between El Niño and La Niña with similar amplitudes. For the low-frequency ENSO mode, however, the west coast year 2 ENSO signal is reduced in magnitude compared to the tide gauges. With the CSEOF decomposition
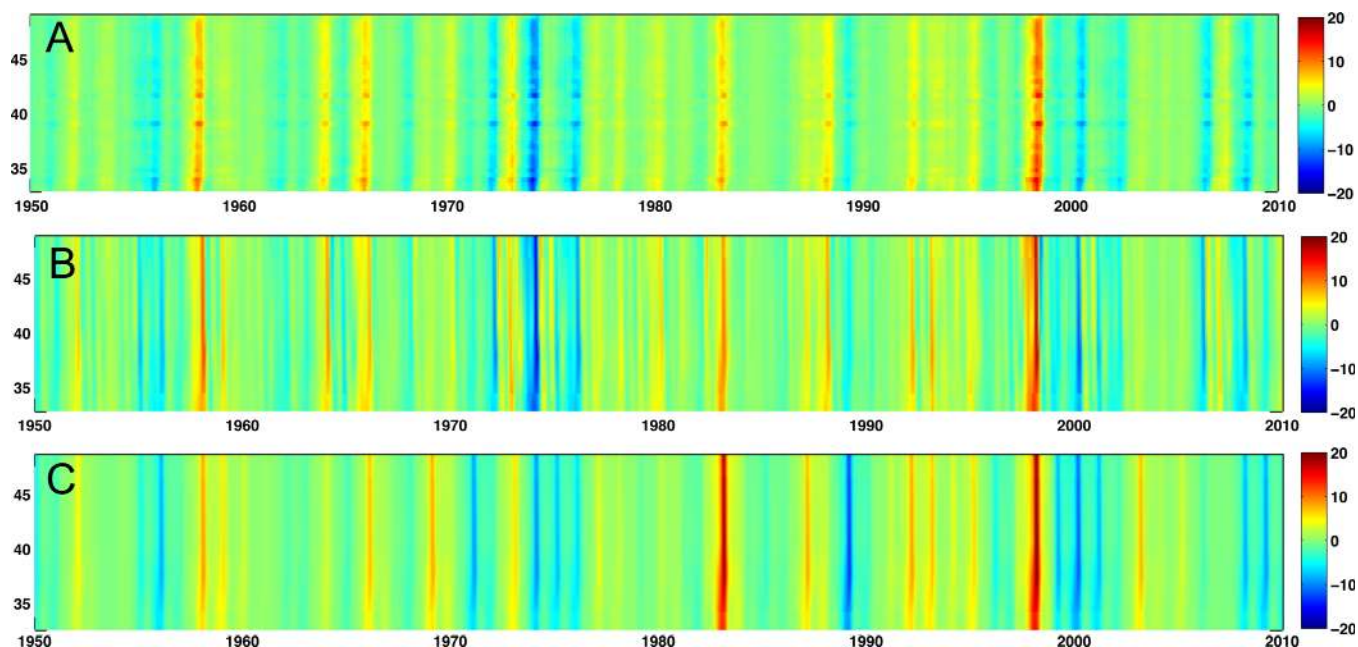
Figure 10. Contribution of ENSO (units of centimeters) to west coast sea level variability from 30°N to 50°N (*y* axis). (a) Contribution of combined 2 year low-frequency (Figure 1) and biennial oscillation (Figure 2) ENSO modes estimated from sea level reconstruction. (b) Contribution of combined 2 year low-frequency (Figure 8) and biennial oscillation (Figure 9) ENSO modes estimated from the tide gauges. (c) Contribution of 1 year ENSO mode (Figure 7) estimated from tide gauges.

starting in 1950, the year 2 JFM map corresponds to JFM of 1983. The reduced amplitude in the reconstruction relative to the tide gauge record suggests the reconstruction may be missing some low-frequency ENSO-related variability. As seen in both the reconstruction and tide gauge data, the contribution of the low-frequency ENSO mode to east coast sea level variability is generally small, suggesting most of the ENSO-related variability on the east coast is a result of the biennial oscillation between El Niño and La Niña (and vice versa).

As a final method of analyzing the difference between the reconstruction and tide gauges, the reconstructed values from the two ENSO modes from within 2° of the west coast of the United States are averaged to create a time series of near-coast ENSO contribution at each latitude (Figure 10a). For comparison, the tide gauge-measured contributions from the 2 year ENSO modes (as seen in Figures 8 and 9; Figure 10b) and the 1 year ENSO mode (as seen in Figure 7; Figure 10c) are also evaluated along the west coast. In the reconstructed ENSO modes (Figure 10a), the amplitude of most ENSO events decreases as the latitude increases. This is not similarly true in the tide gauge analysis. Furthermore, while the amplitudes for the 1997/1998 El Niño agree reasonably well, the effect of the 1982/1983 El Niño on coastal sea level appears to be underestimated by the sea level reconstruction, consistent with the other results above and the study of *Thompson et al*. [2014]. Finally, to underscore the importance of capturing both the low-frequency and biennial ENSO variability, the large La Niña events in the 1970s are estimated to have significantly lower amplitude when using a 1 year CSEOF analysis. In the 2 year analysis of both the reconstruction and tide gauges, the estimated amplitude was larger suggesting that the low-frequency mode that is likely missed by the 1 year analysis contributed significantly to these events.

6. Summary and Discussion

Quantifying the contribution of internal variability and understanding the potential increases and decreases resulting from such variability on local sea levels is important to adaptation and mitigation efforts. As discussed in this paper, sea level can change on the order of tens of centimeters on very short time scales (~1 year). For comparison, the recent IPCC AR5 report [*Church et al*., 2013] projects global sea level to rise by a similar amount by 2100 when considering the secular trend associated with anthropogenic warming. While

this ENSO-related sea level variability has already been observed and experienced over the past 60 years, as underlying sea level continues to rise as a result of anthropogenic warming, the impacts and consequences of this interannual-to-decadal sea level change will be amplified. The contribution of ENSO and other internal variability in the coastal tide gauges must be accounted for when projecting future sea level changes and designing efforts to mitigate the effects of rising sea levels.

To date, sea level reconstructions have seen little use for near-coast applications. Understanding how the reconstruction relates to sea level measured at the tide gauges and represents sea level at coastlines with few or no tide gauges has important implications for the role of reconstructions in coastal planning efforts. Assessing future sea level impacts needs to include an assessment of the contribution of internal variability like ENSO in addition to contributions from anthropogenic sea level rise, tides, and storm surge, to name just a few. As seen in Figure 6, the amplitude of the ENSO-related variability appears to be larger than that estimated from both the satellite altimetry data and sea level reconstruction. It is possible that other regions not considered as part of this study could have even larger differences. While it is possible that this discrepancy is related to problems in the underlying satellite altimetry data near the coast, it is more likely that the tide gauge-measured sea level variability is affected by higher-frequency variability [e.g., *Subbotina et al.*, 2001; *Thompson et al.*, 2013] that is difficult to capture in the altimeter-based sea level reconstruction. Estimates of the near-coast ENSO variability from the sea level reconstruction still provide valuable information regarding how the deep ocean ENSO signal is related to coastal sea level variability. These estimates also provide a reasonable lower bound on the possible contribution of ENSO to coastal sea level. To create reconstructions that more accurately reflect the actual sea level response at the coast, however, will likely take improvements and refinements in the reconstruction approach. This could include adopting an improved underlying satellite altimeter product providing better measurements near the coast, or substituting actual tide gauge measurements back into the reconstruction, similar to what has been done for precipitation reconstructions [*Smith et al.*, 2012]. Additionally, it is possible that reconstructing only specific regions of interest as opposed to performing global reconstructions could lead to improvements in the ability to capture regional internal variability. In general, sea level reconstructions are global in scale, so considering the performance of such reconstructions on regional levels as done here is important in evaluating their usefulness on smaller scales.

By separating the ENSO-related sea level variability into a low-frequency mode and a biennial mode using CSEOFs, a better understanding of how ENSO affects sea level can be gained. The phasing of the two components of ENSO becomes important when considering the impact of future ENSO events. These two modes also provide the opportunity to improve the understanding of the relationship between the Pacific Decadal Oscillation and ENSO. The first CSEOF mode appears to link the variability in the north Pacific to that in tropical Pacific, suggesting that the PDO is related to (or simply is) low-frequency ENSO variability. Furthermore, by improving our physical interpretation and accounting for a portion of the sea level variability in the reconstructed and satellite altimetry sea level data sets, it is possible to remove this sea level variability and gain a better understanding of the underlying signal that is related to anthropogenic warming. This is particularly relevant for the U.S. west coast that has experienced a well-documented lack of sea level rise in the past 20 years, due in large part to internal variability [e.g., *Bromirski et al.*, 2011]. While this study focuses on Pacific Ocean variability, similar studies could be conducted on other types of internal variability in other parts of the global ocean. This study, however, demonstrates how advanced analysis techniques like CSEOFs can be combined with the longer data record from the sea level reconstruction to estimate the potential impacts of an important component of future regional sea level change. Although much of the focus on future sea level rise concerns the long-term trend associated with anthropogenic warming, on shorter time scales, internal climate variability can contribute significantly to regional sea level. Such sea level variability should be taken into consideration when planning efforts to mitigate the effects of future sea level change. In this study, we quantify the contribution to regional sea level of the El Niño-Southern Oscillation (ENSO). Through cyclostationary empirical orthogonal function analysis (CSEOF) of the long reconstructed sea level data set and tide gauges, two global modes dominated by Pacific Ocean variability are identified and related to ENSO and, by extension, the Pacific Decadal Oscillation. By estimating the combined contribution of these two modes to regional sea level, we find that ENSO can contribute up to half a meter of sea level change on short time scales in some locations, with contributions of up to 20 cm along the west coast of the U.S. Tandem analyses of both the reconstructed and tide gauge records also examine the utility of the sea level reconstructions for near-coast studies, and based on the results here, further work is required to provide a better representation of coastal sea level in global sea level reconstructions.

References

Barnett, T. P., D. W. Pierce, M. Latif, D. Dommenget, and R. Saravanan (1999), Interdecadal interactions between the tropics and midlatitudes in the Pacific Basin, *Geophys. Res. Lett.*, *26*(5), 615–618.

Bromirski, P. D., A. J. Miller, R. E. Flick, and G. Auad (2011), Dynamical suppression of sea level rise along the Pacific Coast of North America: Indications for imminent acceleration, *J. Geophys. Res.*, *116*, C07005, doi:10.1029/2010JC006759.

Cazenave, A., and W. Llovel (2010), Contemporary sea level rise, *Annu. Rev. Mar. Sci.*, *2*, 145–173.

Chambers, D. P., C. A. Melhaff, T. J. Urban, D. Fuji, and R. S. Nerem (2002), Low-frequency variations in global mean sea level: 1950–2000, *J. Geophys. Res.*, *107*(C4), 3026, doi:10.1029/2001JC001089.

Chelton, D. B., and R. E. Davis (1982), Monthly mean seal-level variability along the west coast of North America, *J. Phys. Oceanogr.*, *12*, 757–784.

Church, J. A., and N. J. White (2006), A 20th century acceleration in global sea level rise, *Geophys. Res. Lett.*, *33*, L01602, doi:10.1029/2005GL024826.

Church, J. A., and N. J. White (2011), Sea-level rise from the late 19th to the early 21st century, *Surv. Geophys.*, *32-34*, 585–602.

Church, J. A., N. J. White, R. Coleman, K. Lambeck, and J. X. Mitrovica (2004), Estimates of the regional distribution of sea level rise over the 1950–2000 period, *J. Clim.*, *17*, 2609–2625.

Church, J. A., et al. (2013), *Climate Change: The Physical Science Basis, Contribution of Working Group I to the Fifth Assessment Report of the Intergovernmental Panel on Climate Change*, edited by T. F. Stocker et al., chap 13, Cambridge Univ. Press, Cambridge, U. K.

Compo, G. P., and P. D. Sardeshmukh (2010), Removing ENSO-related variations from the climate record, *J. Clim.*, *23*, 1957–1978.

Cooper, M. J. P., M. D. Beevers, and M. Oppenheimer (2008), The potential impacts of sea level rise on the coastal region of New Jersey, USA, *Clim. Change*, *90*, 475–92.

Cummins, P. F., G. S. E. Lagerloef, and G. Mitchum (2005), A regional index of northeast Pacific variability based on satellite altimeter data, *Geophys. Res. Lett.*, *32*, L17607, doi:10.1029/2005GL023642.

Enfield, D. B., and J. S. Allen (1980), On the structure and dynamics of monthly mean sea level anomalies along the Pacific coast of North and South America, *J. Phys. Oceanogr.*, *10*, 557–578.

Gu, D., and S. G. Philander (1997), Interdecadal climate fluctuations that depend on exchanges between the tropics and extratropics, *Science*, *275*(5301), 805–807.

Hamlington, B. D., R. R. Leben, R. S. Nerem, and K.-Y. Kim (2011a), The effect of signal-to-noise ratio on the study of sea level trends, *J. Clim.*, *24*, 1396–1408.

Hamlington, B. D., R. R. Leben, R. S. Nerem, W. Han, and K.-Y. Kim (2011b), Reconstruction sea level using cyclostationary empirical orthogonal functions, *J. Geophys. Res.*, *116*, C12015, doi:10.1029/2011JC007529.

Hamlington, B. D., R. R. Leben, M. W. Strassburg, R. S. Nerem, and K.-Y. Kim (2013), Contribution of the Pacific decadal oscillation to global mean sea level trends, *Geophys. Res. Lett.*, *40*, 5171–5175, doi:10.1002/grl.50950.

Hamlington, B. D., M. W. Strassburg, R. R. Leben, W. Han, R. S. Nerem, K.-Y. Kim (2014a), Uncovering an anthropogenic sea-level rise signal in the Pacific Ocean, *Nat. Clim. Change*, *4*, 782–785.

Hamlington, B. D., R. R. Leben, M. W. Strassburg, and K.-Y. Kim (2014b), Cyclostationary empirical orthogonal function sea-level reconstruction, *Geosci. Data J.*, *1*, 13–19, doi:10.1002/gdj3.6.

Holgate, S. J., A. Matthews, P. L. Woodworth, L. J. Rickards, M. E. Tamisiea, E. Bradshaw, P. R. Foden, K. M. Gordon, S. Jevrejeva, and J. Pugh (2013), New data systems and products at the permanent service for mean sea level, *J. Coastal Res.*, *29*(3), 493–504, doi:10.2112/JCOASTRES-D-12-00175.1.

Kim, K.-Y. (2002), Investigation of ENSO variability using cyclostationary EOFs of observational data, *Meteorol. Atmos. Phys.*, *81*(3), 149–168.

Kim, K.-Y., and G. R. North (1997), EOFs of harmonizable cyclostationary processes, *J. Atmos. Sci.*, *54*(19), 2416–2427.

Kim, K.-Y., G. R. North, and J. Huang (1996), EOFs of one-dimensional cyclostationary time series: Computations, examples, and stochastic modeling, *J. Atmos. Sci.*, *53*(7), 1007–1017.

Kirshen, P., K. Knee, and M. Ruth (2008), Climate change and coastal flooding in Metro Boston: Impacts and adaptation strategies, *Clim. Change*, *90*, 453–473.

Kleeman, R., J. McCreary, and B. Klinger (1999), A mechanism for generating ENSO decadal variability, *Geophys. Res. Lett.*, *26*(12), 1743–1746.

Latif, M., R. Kleeman, and C. Eckert (1997), Greenhouse warming, decadal variability, or El Niño? An attempt to understand the anomalous, *J. Clim.*, *10*(9), 2221–2239.

Mantua, N. J., and S. R. Hare (2002), The Pacific decadal oscillation, *J. Oceanogr.*, *58*, 35–44.

Mantua, N. J., S. R. Hare, Y. Zhang, J. M. Wallace, and R. C. Francis (1997), A Pacific interdecadal climate oscillation with impacts on salmon production, *Bull. Am. Meteorol. Soc.*, *78*, 1069–1079.

Merrifield, M. A., P. Thompson, and M. Lander (2012), Multidecadal sea level anomalies and trends in the western tropical Pacific, *Geophys. Res. Lett.*, *39*, L13602, doi:10.1029/2012GL052032.

Meyssignac, B., D. Salas y Melia, M. Becker, W. Llovel, and A. Cazenave (2012), Tropical Pacific spatial trend patterns in observed sea level: Internal variability and/or anthropogenic signature?, *Clim. Past*, *8*, 787–802.

Mitchum, G. T., R. S. Nerem, M. A. Merrifield, and W. R. Gehrels (2010), Modern sea-level-change estimates, in *Understanding Sea-level Rise and Variability*, edited by J. A. Church et al., pp. 122–142, John Wiley, Chichester, U. K.

Moon, J.-H., Y. T. Song, P. D. Bromirski, and A. J. Miller (2013), Multi-decadal regional sea level shifts in the Pacific over 1958–2008, *J. Geophys. Res. Oceans*, *118*, 7024–7035, doi:10.1002/2013JC009297.

Pierce, D. W., T. P. Barnett, and M. Latif (2000), Connections between the Pacific Ocean tropics and midlatitudes on decadal timescales, *J Clim.*, *13*(6), 1173–1194.

Rasmusson, E. M., X. Wang, and C. F. Ropelewski (1990), The biennial component of ENSO variability, *J. Mar. Syst.*, *1*(1), 71–96.

Saji, N. H., B. N. Goswami, P. N. Vinayachandran, and T. Yamagata (1999), A dipole mode in the tropical Indian Ocean, *Nature*, *401*, 360–363, doi:10.1038/43855.

Smith, T. M., R. W. Reynolds, T. C. Peterson, and J. Lawrimore (2008), Improvements NOAAs historical merged land–ocean temp analysis (1880–2006), *J. Clim.*, *21*, 2283–2296.

Smith, T. M., P. A. Arkin, L. Ren, and S. P. Shen (2012), Improved reconstruction of global precipitation since 1900, *J. Atmos. Oceanic Technol.*, *29*(10), 1505–1517.

Subbotina, M. M., R. E. Thomson, and A. B. Rabinovich (2001), Spectral characteristics of sea level variability along the west coast of North America during the 1982–83 and 1997–98 El Niño events, *Prog. Oceanogr.*, *49*(1-4), 353–372.

Suzuki, R., S. K. Behera, S. Iizuka, and T. Yamagata (2004), Indian Ocean subtropical dipole simulated using a coupled general circulation model, *J. Geophys. Res.*, *109*, C09001, doi:10.1029/2003JC001974.

Sweet, W. V., and J. Park (2014), From the extreme to the mean: Acceleration and tipping points of coastal inundation from sea level rise, *Earth's Future*, *2*, 579–600, doi:10.1002/2014EF000272.

Sweet, W. V., and C. Zervas (2011), Cool-Season sea level anomalies and storm surges along the U.S. East Coast: Climatology and comparison with the 2009/10 El Niño, *Mon. Weather Rev.*, *139*(7), 2290–2299.

Tebaldi, C., B. H. Strauss, and C. E. Zervas (2012), Modelling sea level rise impacts on storm surges along US coasts, *Environ. Res. Lett.*, *7*, 014032.

Thompson, P. R., and G. T. Mitchum (2014), Coherent sea level variability on the North Atlantic western boundary, *J. Geophys. Res. Oceans*, *119*, 5676–5689, doi:10.1002/2014JC009999.

Thompson, P. R., G. T. Mitchum, C. Vonesch, and J. Li (2013), Variability of winter storminess in the Eastern United States during the twentieth century from tide gauges, *J. Clim.*, *26*, 9713–9726.

Thompson, P. R., M. A. Merrifield, J. R. Wells, and C. M. Chang (2014), Wind-Driven coastal sea Level variability in the Northeast Pacific, *J. Clim.*, *27*, 4733–4751.

Vimont, D. J., J. M. Wallace, and D. S. Battisti (2003), The seasonal footprinting mechanism in the Pacific: Implications for ENSO, *J. Clim.*, *16*, 2668–2675.

Vinogradov, S. V., and R. M. Ponte (2011), Low-frequency variability in coastal sea level from tide gauges and altimetry, *J. Geophys. Res.*, *116*, C07006, doi:10.1029/2011JC007034.

Wahl, T., F. M. Calafat, and M. E. Luther (2014), Rapid changes in the seasonal sea level cycle along the US Gulf coast from the late 20th century, *Geophys. Res. Lett.*, *41*, 491–498.

Wolter, K., and M. S. Timlin (2011), El Niño/Southern Oscillation behaviour since 1871 as diagnosed in an extended multivariate ENSO index (MEI.ext), *Int. J. Climatol.*, *31*, 1074–1087, doi:10.1002/joc.2336.

Woodworth, P. L., N. J. White, S. Jevrejeva, S. J. Holgate, J. A. Church, and W. R. Gehrels (2009), Evidence for the accelerations of sea level on multi-decade and century timescales, *Int. J. Climatol.*, *29*, 777–789.

Woodworth, P. L., M. A. Morales Maqueda, V. M. Roussenov, R. G. Williams, and C. W. Hughes (2014), Mean sea-level variability along the northeast American Atlantic coast and the roles of the wind and the overturning circulation, *J. Geophys. Res. Oceans*, *119*, 8916–8935, doi:10.1002/2014JC010520.

Yeo, S.-R., and K.-Y. Kim (2014), Global warming, low-frequency variability and biennial oscillation: An attempt to understand the physical mechanisms driving major ENSO events, *Clim. Dyn.*, *43*, 771–786, doi:10.1007/s00382-013-1862-1.

Zhang, X., and J. A. Church (2012), Sea level trends, interannual and decadal variability in the Pacific Ocean, *Geophys. Res. Lett.*, *39*, L21701, doi:10.1029/2012GL053240.